Experimental and Chemical Kinetic Modeling Study of 3-Pentanone Oxidation

Z. Serinyel,[†] N. Chaumeix,[‡] G. Black,[†] J. M. Simmie,[†] and H. J. Curran*[,†]

Combustion Chemistry Centre, School of Chemistry, NUI, Galway, Ireland, and ICARE, CNRS, Orléans, France

Received: July 30, 2010; Revised Manuscript Received: October 4, 2010

Shock tube ignition delay times have been measured for 3-pentanone at a reflected shock pressure of 1 atm (±2%), in the temperature range 1250−1850 K, at equivalence ratios of 0.5−2.0 for O_2 mixtures in argon with fuel concentrations varying from 0.875 to 1.3125%. Laminar flame speeds have also been measured at an initial pressure of 1 atm over an equivalence ratio range. Complementary to previous studies [Pichon S., Black, G., Chaumeix, N., Yahyaoui, M., Simmie, J. M., Curran, H. J., Donohue, R. *Combust. Flame*, **2009**, *156*, 494−504; Serinyel, Z.; Black, G.; Curran, H. J.; Simmie, J. M. *Combustion Sci. Tech.*, **2010**, 182, 574−587], laminar flame speeds of 2-butanone have also been measured, and relative reactivities of these ketones have been compared and discussed. A chemical kinetic submechanism describing the oxidation of 3-pentanone has been developed and detailed in this paper; rate constants for unimolecular fuel decomposition reactions have been treated for falloff in pressure with nine-parameter fits using the Troe Formulism. Both compounds treated in this work may be used as fuel tracers, thus further ignition delay time measurements have been carried out by adding 3-pentanone to *n*-heptane in order to test the effect of the blend on ignition delay timing. It was found that the autoignition characteristics of n-heptane remained unaffected in the presence of 15% 3-pentanone in the fuel, consistent with results obtained using acetone and 2-butanone [Pichon S., Black, G., Chaumeix, N., Yahyaoui, M., Simmie, J. M., Curran, H. J., Donohue, R. *Combust. Flame*, **2009**, *156*, 494−504; Serinyel, Z.; Black, G.; Curran, H. J.; Simmie, J. M. *Combustion Sci. Tech.*, **2010**, 182, 574−587].

Introduction

To optimize the performance of combustion systems, it is important to understand the physical and chemical effects experienced during the combustion process, such as the actual location of the fuel within the combustion chamber, the temperature field, etc. Laser imaging diagnostics have been developed as a non-invasive, near-instantaneous tool for monitoring fuel, equivalence ratio, and temperature distribution in combustion systems and ketones are often used as fuel tracers due to their ability to fluoresce at conveniently available accessible excitation wavelengths.[3]

Ketones absorb in the ultraviolet region due to the $n \rightarrow \pi^*$ transition of the carbonyl group. Thus, 3-pentanone (diethyl ketone) fluorescence has been studied in terms of its dependence of temperature, pressure, bath gas concentration,[4,5] and excitation wavelength.[6] Berckmüller et al.[4] showed that acetone (dimethyl ketone), 2-butanone (methyl ethyl ketone), and 3-pentanone could all be used to quantify fuel concentration in a spark-ignition engine due to the positive dependence of their relative fluorescence on temperature. Due to its similar diffusive and evaporative properties to iso-octane, 3-pentanone has been used as a fuel tracer in internal combustion engine applications; Einecke et al.[7] doped iso-octane with 3-pentanone to measure the temperature field in a single cylinder two-stroke engine using planar Laser Induced Fluorescence (LIF). Neij et al.[8] used 3-pentanone in order to map iso-octane fuel distribution at ignition in a spark ignition engine using LIF. Han and Steeper and Rothamer et al.[9,10] used these three ketones along with 3-hexanone to develop a technique to quantify equivalence ratio in internal combustion engines. Fuel tracers are usually added to the fuel in quantities of up to 15%. It is important that the presence of the tracer does not affect the oxidation characteristics of the fuel.

Despite all of this work relating to fluorescence, the oxidation chemistry of ketones and their ignition characteristics are not well-known; compared to the relatively high number of experimental studies concerning oxygenated fuels such as alcohols and esters, fewer studies exist on this family.[1,2,12,13]

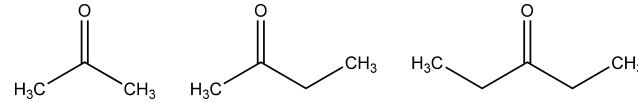

In this study, ignition delay times for 3-pentanone oxidation recorded in a shock tube and laminar flame speed measurements of 2-butanone and 3-pentanone performed on outwardly propagating spherical flames generated in a spherical bomb will be described. Thereafter, the development of a detailed chemical kinetic submechanism will be discussed, along with comparisons of simulations to the experimental data.

Experimental Section

1. Shock Tube Ignition Delay Measurements. Ignition delay measurements were carried out in the low-pressure shock tube facility at the Combustion Chemistry Centre, Galway, which is described in detail elsewhere.[14] It consists of a test section measuring 6.22 m in length, with an internal diameter of 10.24 cm, and a barrel-shaped driver section measuring 53

* To whom correspondence should be addressed. E-mail: henry.curran@nuigalway.ie.
[†] NUI Galway.
[‡] CNRS.

10.1021/jp107167f
Published on Web 10/29/2010

TABLE 1: Shock Tube Mixture Compositions for 3-Pentanone in Molar Percent

mixture No.	fuel %	O_2 %	Ar %	φ
1	0.875	3.063	96.063	2.00
2	1.250	5.000	93.750	1.75
3	1.313	6.125	92.563	1.50
4	0.875	6.125	93.000	1.00
5	0.875	12.25	86.875	0.50
6	0.438	6.125	93.437	0.50

cm in length. The two sections are separated by a polycarbonate diaphragm, which petals when forced into contact with a cross-shaped cutter due to the pressure differential between the high-pressure driver section and the low-pressure test section. The driver gas used was helium (99.99% pure; BOC).

3-Pentanone was obtained in 99%+ purity (Aldrich) and was dried before use over a molecular sieve. Mixtures were prepared manometrically, see Table 1, and care was taken that the maximum 3-pentanone pressure utilized was well below the room temperature saturation vapor pressure, 28.1 Torr at 20 °C.

Light emission from CH* at 431 nm was detected through a fused silica window embedded in the end plate using a photodetector (Thorlabs Inc. PDA55-EC) and a narrow band-pass filter centered at 431 nm with a full-width half-maximum of 10 nm. Time counters located along the last half meter of the test section determine the velocity of the incident shock wave. The velocity at the end-wall was determined through linear extrapolation, so as to take attenuation of the shock wave into account. This value was then used to calculate the temperature and pressure of the mixture behind the reflected shock wave, using the application Gaseq,[15] which solves the mass, energy, and momentum conservation equations together with the ideal gas law. The pressure at the end-wall was monitored by means of an in situ pressure transducer (Kistler, model 603B). The ignition delay time was defined as the interval between the rise in pressure due to the arrival of the shock wave at the end-wall and the maximum rate of rise of the light emission signal.

Ignition delay times for acetone[1] and 2-butanone have been published previously.[2] A regression analysis will be given in this paper in order to highlight the differences they exhibit in terms of reactivity.

2. Laminar Flame Speed Measurements. Flame speed measurements were carried out in a spherical bomb consisting of a stainless steel sphere with a black polished inner surface and an internal diameter of 476 mm. Two stainless steel electrodes protrude diametrically into the center of the bomb, leaving an adjustable gap of approximately 1 mm between them. These electrodes are connected to a high voltage source to generate a spark and thereby induce ignition at the center of the bomb. The energy deposited by the spark is measured as being approximately 2 mJ. Optical access is provided by two facing quartz windows, 100 mm in diameter and 50 mm thick. The optical system used to visualize the flame is a Schlieren setup consisting of a xenon lamp (Jobin Yvon), two lenses (150 and 22 mm focal length respectively), and two spherical concave mirrors (250 mm diameter, 1 m focal length) situated on either side of the bomb.

The image of the flame front is projected onto a viewing screen, where it is recorded using a high speed camera (Photron, Fastcam APX model 120K). Flush with the inner surface of the spherical bomb, a pressure transducer (Kistler 601A), equipped with a flame arrestor (Kistler 6505), is mounted in order to monitor the pressure evolution inside the bomb during combustion and thereby derive the maximum pressure at the end of combustion. The signal delivered by the pressure transducer is recorded along with the voltage between the electrodes and a TTL signal delivered by a delay generator. This generator synchronizes the camera and the digital oscilloscope with the spark fixing the same initial time to all the devices.

Following spark ignition, a spherical flame which expands outwardly is produced, Figure 1. Depending on the equivalence ratio, the flame can exhibit a very smooth surface as it grows (Figure 1a) or can present a wrinkled surface as is shown in Figure 1b. The relationship between the laminar flame speed and the growth of the flame assumes that the flame is smooth, which means that the envelope of the flame-ball is the flame; however, in the case of a wrinkled flame, this hypothesis is no longer valid. Therefore, laminar flame speed is derived only

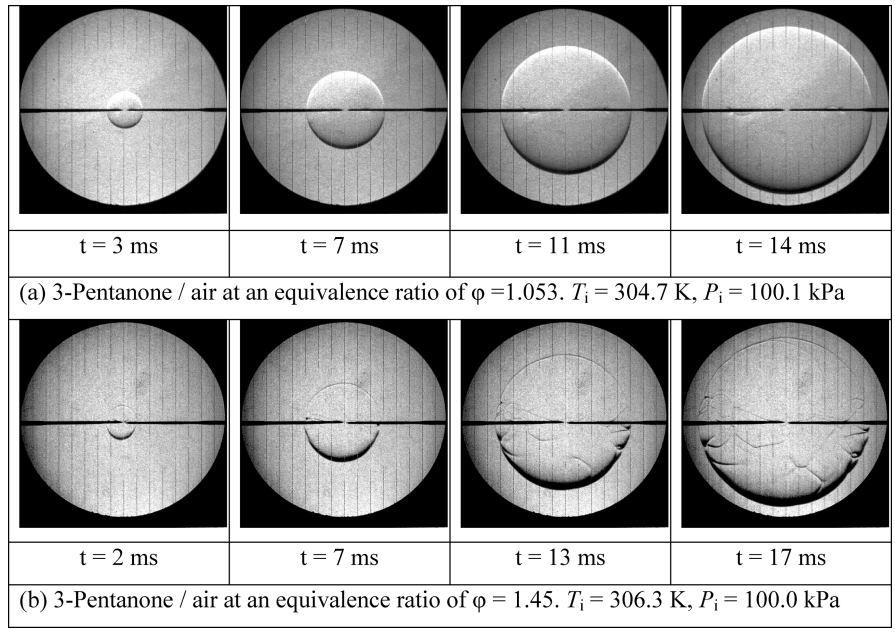

Figure 1. Schlieren snapshot images of flame propagation for 3-pentanone/air flame at two different equivalence ratios. (a) Smooth flame; (b) wrinkled flame.

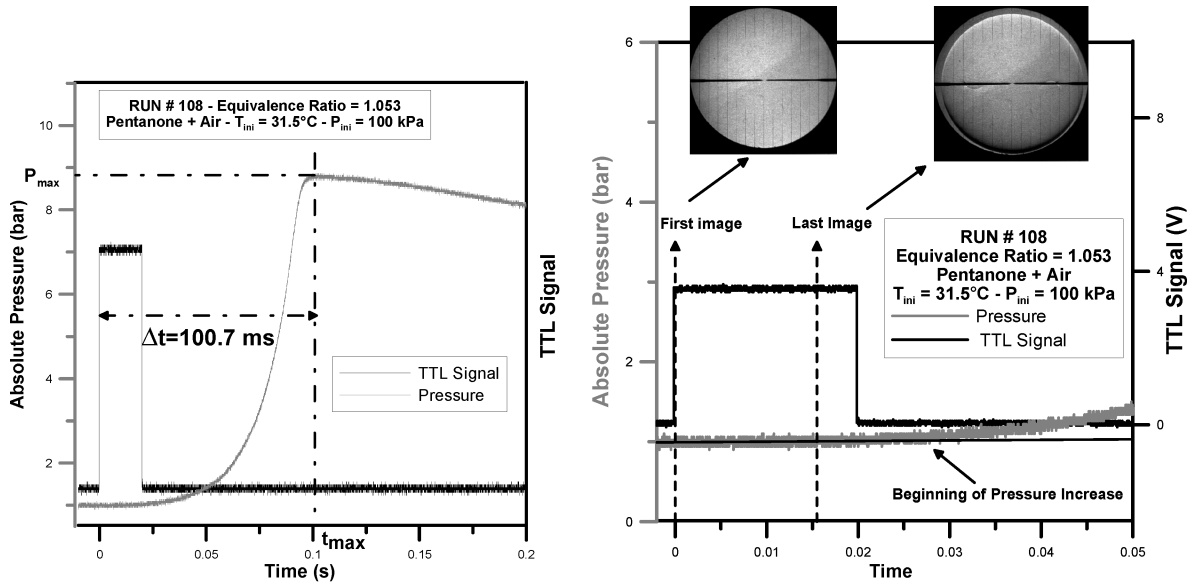

Figure 2. Evolution of the pressure inside the vessel during combustion for a mixture of 3-pentanone/air at an equivalence ratio of $\varphi = 1.053$. The mixture was initially at ambient temperature and 100.1 kPa. (a) Full recording time; (b) zoom around the observation time.

TABLE 2: Mixture Mole Fractions for Freely Propagating Flame Study

2-butanone	O_2	N_2	φ	3-pentanone	O_2	N_2	φ
0.0279	0.2038	0.7668	0.750	0.0220	0.2051	0.7715	0.750
0.0280	0.2038	0.7667	0.753	0.0232	0.2048	0.7703	0.792
0.0297	0.2034	0.7654	0.802	0.0249	0.2045	0.7692	0.850
0.0314	0.2032	0.7642	0.849	0.0263	0.2041	0.7679	0.899
0.0332	0.2027	0.7627	0.898	0.0272	0.2040	0.7676	0.933
0.0332	0.2027	0.7626	0.899	0.0274	0.2040	0.7673	0.939
0.0351	0.2024	0.7613	0.952	0.0283	0.2038	0.7665	0.969
0.0373	0.2019	0.7595	1.013	0.0292	0.2035	0.7657	1.001
0.0386	0.2016	0.7583	1.052	0.0305	0.2032	0.7645	1.050
0.0395	0.2014	0.7577	1.078	0.0306	0.2033	0.7647	1.053
0.0400	0.2012	0.7571	1.090	0.0313	0.2031	0.7642	1.076
0.0402	0.2011	0.7566	1.098	0.0328	0.2028	0.7629	1.130
0.0403	0.2012	0.7570	1.099	0.0333	0.2027	0.7625	1.148
0.0404	0.2012	0.7568	1.102	0.0339	0.2025	0.7619	1.170
0.0410	0.2011	0.7565	1.118	0.0349	0.2025	0.7616	1.204
0.0420	0.2009	0.7556	1.150	0.0361	0.2021	0.7603	1.248
0.0421	0.2008	0.7555	1.150	0.0361	0.2021	0.7601	1.248
0.0438	0.2005	0.7542	1.200	0.0375	0.2019	0.7594	1.297
0.0455	0.2001	0.7529	1.248	0.0389	0.2015	0.7581	1.348
0.0472	0.1998	0.7516	1.298	0.0389	0.2015	0.7579	1.350
0.0473	0.1998	0.7517	1.299	0.0402	0.2011	0.7567	1.397
0.0491	0.1994	0.7500	1.351	0.0417	0.2009	0.7558	1.450
0.0507	0.1990	0.7488	1.398				

within the domain of equivalence ratio for which the flame is smooth or for which there is very limited wrinkling.[16]

The evolution of pressure with time is plotted in Figure 2, where the maximum pressure achieved at the end of combustion is derived and can be compared to the theoretical value deduced from an equilibrium calculation assuming adiabatic combustion at constant volume, P_{AICC}. The rise of the TTL signal, illustrated in Figure 2, indicates the onset of combustion and thus corresponds to the first camera image recorded.

Within the camera observation time, from ignition to the image where the flame reaches the optical diameter, it is important to monitor the pressure inside the vessel so that, during this time interval, the pressure is constant and equal to its initial value. In Figure 2b, the evolution of pressure during this time interval is reported as well as the first and last images. As one can see, the last image of the flame was taken at a time of 15.5 ms, while the pressure rise did not begin until much later, at times of approximately 28−29 ms.

The combustible mixture was obtained by vaporizing 2-butanone (Sigma-Aldrich, +99%) or 3-pentanone (Sigma-Aldrich, 99%+) directly into the bomb at the desired partial pressure, then dry laboratory air was added up to the total pressure of 100 kPa. The mixture was allowed to rest for several minutes before ignition. The mixture compositions tested in the spherical bomb are presented in Table 2.

The images recorded by the high speed camera are processed using an in-house code that extracts the radius of the flame. The time evolution of the radius is given in Figure 3 for different equivalence ratios, where the variation is quasi-linear for all four mixtures.

From the evolution of the radius versus time, one can extract the spatial flame speed defined as:

$$V_S = \frac{dr_{fl}}{dt} \quad (1)$$

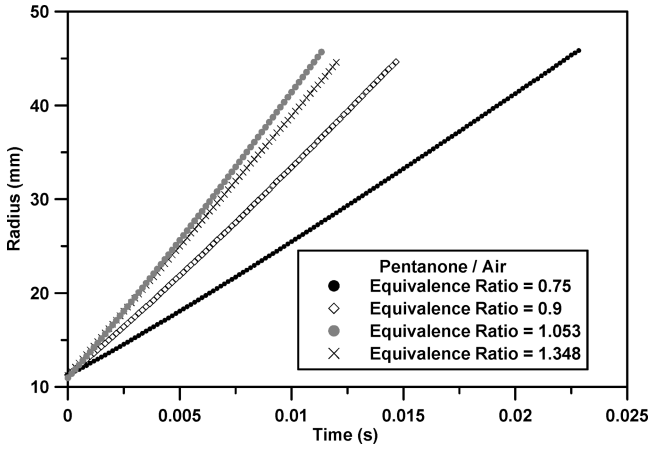

Figure 3. Evolution of the measured radius as a function of time for different mixtures of 3-pentanone/air initially at 100 kPa.

Eschenbach and Agnew[17] have shown that, in the case of expanding flames the spatial flame velocity is linked to the laminar flame velocity through the following expression:

$$S_L = \left(V_S + \frac{r_b}{3 \cdot P_b}\frac{dP_b}{dt}\right)\left(\frac{M_b}{M_u}\right)\left(\frac{T_u}{T_b}\right)\left(\frac{P_b}{P_u}\right) \quad (2)$$

where S_L is the laminar flame velocity, V_S is the spatial flame velocity, r is the radius of the flame, M is the molecular weight, T is the temperature, P is the pressure, and the subscripts u and b represent the unburned and burned conditions, respectively.

When the flame development is limited such that no pressure increase is induced, a simple relationship exists between the spatial flame velocity, V_S, and the laminar flame speed, S_L, if the expansion ratio, σ, is known:

$$S_L = \frac{V_S}{\sigma} \quad (3)$$

$$\sigma = \left(\frac{M_b}{M_u}\right)\left(\frac{T_u}{T_b}\right)\left(\frac{P_b}{P_u}\right) = \frac{\rho_u}{\rho_b} \quad (4)$$

Owing to its spherical shape, the flame is stretched and hence its velocity differs from that of an ideal planar one. A spherical flame is the subject of a local stretch, and the apparent velocity is the stretched one ($V_S = (dr_f/dt)$), where r_f is the flame radius and t is the time. It differs from the unstretched velocity, V_s^0, by a coefficient known as the Markstein length, L, as long as the stretch rate, κ, is weak and the Zeldovich number, β, is large: $V_S = V_S^0 - L\kappa$. In the case of a spherical expanding flame, the stretch rate, κ, is given by: $\kappa = 2V_S/R_f$.[19–22] Then, the unstretched spatial flame velocity, V_s^0, is determined by the integrated form:[23,24]

$$\frac{r_f}{r_{final}} = V_S^0 \times (t_{final} - t) - 2L \times \ln\left(\frac{r_f}{r_{final}}\right) \quad (5)$$

where V_s^0 is the unstretched spatial velocity, L is the Markstein length, r is the flame radius, r_{final} is the final flame radius measured, t is time, and t_f is the final time measured.

A regression analysis was performed in order to derive both V_s^0 and L with a coefficient of determination r^2 better than 0.9999. The unstretched laminar flame velocity, S_l^0, is then derived from the value of the unstretched spatial flame velocity, V_s^0, and the expansion factor, σ, which is evaluated using the adiabatic flame calculation of the application COSILAB.[25]

TABLE 3: Thermodynamic Properties for Selected Species in 3-Pentanone Oxidation

species	H_f°(298 K), kcal/mol	S°(298 K), cal/(mol K)	C_p(300 K), cal/(mol K)
$C_2H_5COC_2H_5$	−62.20	92.25	30.37
$C_2H_5COC_2H_4p$	−13.20	95.46	36.04
$C_2H_5COC_2H_4s$	−18.25	91.69	37.59
$C_2H_5COCH_2$	−14.60	80.72	24.38

Chemical Kinetic Model. The 2-butanone submechanism was developed in a previous study,[2] therefore we do not explain it in detail here. The submechanism of C2−C3 hydrocarbon chemistry is the same as the recent natural gas[26–30] and both *n*- and *iso*-butane[31–33] mechanisms and their blends published from this laboratory. The 3-pentanone submechanism has been developed and integrated into a previously established and recently revised C4 mechanism, which is available on the web page of the Combustion Chemistry Centre at NUI Galway.[34] Thermodynamic properties of the fuel and primary fuel radical species resulting from hydrogen abstraction from 3-pentanone have been calculated using THERM[35] using group additivity and are given in Table 3. Thermodynamic properties for all species involved in the oxidation of 3-pentanone, together with a full list of thermodynamic properties of the fuel and fuel radicals, in NASA polynomial format can also be found on the Web site.[34] Unimolecular fuel decomposition, hydrogen abstraction and decomposition of the resulting fuel radicals will be discussed separately.

Unimolecular Decomposition Reactions. The rate constant for unimolecular decomposition reactions are estimated in the reverse direction and assuming the high pressure limit value. The radical−radical recombination of R1 and R2 to form the fuel are assigned rate constants of $3.13 \times 10^{14} \times T^{-0.5}$ s^{-1} for reaction R1 and $1.93 \times 10^{14} \times T^{-0.32}$ s^{-1} for reaction R2 respectively, based on Tsang's recommendations for ethyl recombination with acetyl and methyl recombination with n-propyl radical,[36,37] respectively.

$$C_2H_5COC_2H_5(+M) \leftrightarrow C_2H_5 + C_2H_5CO(+M) \quad (R1)$$

$$C_2H_5COC_2H_5(+M) \leftrightarrow CH_3 + C_2H_5COCH_2(+M) \quad (R2)$$

These high-pressure limit rate constants were then treated using Quantum Rice-Ramsperger Kassel (QRRK) theory combined with a master equation analysis as described by Dean et al.[38,39] in order to account for pressure falloff effects. This treatment resulted in the generation of rate constant expressions presented in a nine-parameter Troe form.[40] The bath gas in these calculations is argon (as this was used in our experiments), and its efficiency is estimated as 0.7 times that of nitrogen.

Hydrogen Abstraction Reactions. Rate constants for hydrogen abstraction were taken from the work of Orme,[41] who described those for abstraction of hydrogen atoms on 1°, 2°, and 3° carbons in alkanes. However, some changes have been made. For abstraction by hydroperoxyl (HO_2) radical rate constants were taken from the work of Aguilera-Iparraguirre,[42] who used quantum chemistry at a high level of theory to

TABLE 4: Estimated Hydrogen Abstraction Reaction Rate Constants on a Per H-Atom Basis (cm^3 mol s cal K) from 3-Pentanone (α-Hydrogen to the Carbonyl Carbon)

abstraction by	A	n	E_a
OH	1.30×10^3	2.77	−1230
O	7.22×10^{10}	0.23	2970
O_2	1.01×10^{13}	0.00	45850
HO_2	1.72×10^{12}	0.05	17876
H	4.78×10^5	2.29	2875
CH_3O	2.88×10^{11}	0.00	4573
CH_3O_2	1.72×10^{12}	0.05	17876
CH_3	$4.26 \times 10°$	3.28	5267
C_2H_5	1.50×10^{10}	0.00	8600
C_2H_3	1.50×10^{10}	0.00	5600

calculate rates of abstractions from methane, ethane, propane, and *n*- and *iso*-butane. Carstensen and Dean[43] also used quantum chemical calculations to determine rate constants for abstraction from these C_1 to C_4 alkanes by HO_2, CH_3O_2, $C_2H_5O_2$, and other larger alkylperoxyl radicals. Their calculated rate constants for abstraction by HO_2 radical are consistently faster[33] than those calculated by Aguilera-Iparraguirre et al., which are at a higher level of theory and are in better agreement with the available, albeit sparse, experimental data. Thus, we have estimated rate constants of abstraction by CH_3O_2 radical in the following way. Carstensen and Dean showed that the rate constant for abstraction by CH_3O_2 radical decreased relative to HO_2 radical for each type of hydrogen atom (1°, 2°, or 3°), which is consistent with its higher molecular weight. Therefore, we decreased the rate constant calculated by Aguilera-Iparraguirre et al. for HO_2 radical by the same relative amount as that reported by Carstensen and Dean in changing from HO_2 to CH_3O_2 radical and generated three-parameter, non-Arrhenius expressions valid in the temperature range 800−1900 K for each type of hydrogen atom being abstracted. The development of these rate constants are also described and provided in the publications of Healy et al.[32,33] and are given in the detailed chemical kinetic mechanism that is available as Supporting Information.

Hydrogen abstraction from the primary site of 3-pentanone has been estimated by analogy with primary H-atom abstraction rate constants from alkanes, given that the corresponding bond dissociation energy of $C_2H_5COC_2H_5 \rightarrow C_2H_5COC_2H_4p + H$ is equal to that of a 1° alkane C−H bond energy with a value of 101.1 kcal mol^{-1}.[44]

The abstraction reaction rate constants for the carbon−hydrogen bonds α to the carbonyl carbon atom, $C_2H_5COCH-HCH_3$, were estimated by assuming 3-pentanone to be analogous to acetone. First, hydrogen abstraction rate constants for acetone[1] are defined over a temperature range on a per hydrogen atom basis. Then in the same temperature range, abstraction rate constants for a normal alkane were estimated for both primary ($k_{1°}$) and secondary ($k_{2°}$) C−H sites, and their ratio ($k_{1°}/k_{2°}$) was taken as a basis for the estimation of the α-H of 3-pentanone. The resulting reaction rate constants were fit using a three-parameter modified Arrhenius expression, $A \times T^n \times \exp(-E_a/RT)$ over the same temperature range, and the overall rate constant is given for the four equivalent H-atoms. The rate constant for $C_2H_5COC_2H_5 + OH \rightarrow C_2H_5COC_2H_4s + H_2O$ was based on the recent computational work of Zhou et al[59] and is calculated as $5.20 \times 10^3\ T^{2.77} \exp(-1230/RT)$.

Rate constants on a per hydrogen atom basis are given in Table 4.

Fuel Radical Decomposition/Isomerization. The unimolecular decomposition rate constants for the fuel radicals, $C_2H_5COC_2H_4p$ and $C_2H_5COC_2H_4s$, are estimated in the reverse direction. The collision factor of the reaction $C_2H_5CO + C_2H_4 \rightarrow C_2H_5COC_2H_4p$ is taken to be 1.0×10^{11} cm^3 mol^{-1} s^{-1} by analogy with $CH_3CO + C_2H_4 \rightarrow C_2H_4COCH_3$.[45] There is no literature value defining the barrier height for this reaction, therefore it is estimated through a linear fit of an Evans−Polanyi plot correlating activation energies of various radical species to ethylene and to their corresponding heats of reaction by using literature values for the activation energies.[46–49] An activation energy barrier of 8420 cal mol^{-1} has been estimated for the given reaction. The reverse (decomposition) rate constant is then calculated via microscopic reversibility to be $7.17 \times 10^{13}T^{-0.47} \exp(-12\,716/T)$ s^{-1}. The rate constant for the reaction $C_2H_5COC_2H_4s \rightarrow CH_3CHCO + C_2H_5$ is also estimated in the recombination direction by analogy with $C_2H_5 + CH_2CO \rightarrow CH_3CH_2CH_2CO$ according to theoretical work of Huynh and Violi[49] for a methyl butanoate decomposition mechanism, and the forward rate constant is calculated through microscopic reversibility as $1.21 \times 10^{19}T^{0.416} \exp(-21\,500/T)s^{-1}$. The remaining alkyl and alkoxy radical decompositions have previously been established by Curran.[45]

The isomerization reaction of the fuel radicals $C_2H_5COC_2H_4p \rightarrow C_2H_5COC_2H_4s$ is estimated by analogy with the p → s hydrogen shift as described by Matheu et al.;[50] with a rate constant expression of $3.56 \times 10^{10}T^{0.88} \exp(-18\,772/T)$ s^{-1}.

Since this study addresses high temperature oxidation of 3-pentanone, reactions describing the addition of fuel radicals to O_2 have not been considered, given that they would be negligible or unimportant compared to beta scission reactions at temperatures greater than 1200 K. However, it is important to note that these reactions should not be omitted if low/intermediate temperature applications are to be addressed, which is beyond the scope of the present study. A listing of the 3-pentanone submechanism is provided in Table 5.

Results

Ignition Delay Times. Ignition delay time calculations were performed with the SENKIN module of the CHEMKIN-PRO application.[51] Constant volume, constant internal energy, and homogeneous mixtures were assumed behind the reflected shock wave. The temperature and pressure of the mixture behind the reflected shock wave (T_5, P_5) are taken as the initial conditions for the simulations. Computed ignition delays were determined from the maximum product of the concentrations of $^{\bullet}C_2H$ and $^{\bullet}O$,[52] which produces the excited species CH* via the reaction: $^{\bullet}C_2H + {}^{\bullet}O \rightarrow CH^* + CO$.

Shock tube ignition delay times of 3-pentanone/O_2/Ar mixtures and the model predictions are given in Figure 4. At a first glance, we see that rich mixtures ignite slower than lean mixtures, which is consistent with other studies on hydrocarbon fuels at these temperatures and pressures.[55,56] The reflected shock temperatures are in the range of 1250−1850 K, where the overall reactivity is governed by the chain branching reaction $H + O_2 \leftrightarrow O + OH$, and hence reactivity is very sensitive to the concentration of molecular oxygen. Therefore, for a fuel concentration of 0.875%, the mixture with the highest content of O_2 (12.25% O_2, mixture 5) shows the highest reactivity and ignites faster than all others, while mixture 1, which contains 3.063% O_2, ignites slowest. On the other hand, for a fixed O_2 concentration of 6.125%, increased concentration of fuel (0.875% to 1.3115% fuel) increases the inhibiting effect of H-abstraction from the fuel by H radical in the chain branching reaction $H + O_2 \leftrightarrow O + OH$, and results in longer ignition delay times. These trends are captured by the model as well, which shows good performance for all cases except for the lean

TABLE 5: Reaction Rate Constants for 3-Pentanone Submechanism (cm^3 mol s cal K)

reaction		A	n	E_a
$C_2H_5COC_2H_5(+M) \leftrightarrow C_2H_5 + C_2H_5CO(+M)$	k_{inf}	1.78×10^{19}	−0.73	81 910
	k_0	1.61×10^{104}	−24.67	105 300
α,T^{***},T^* and T^{**}		$0.90/1.0 \times 10^{10}/5.0 \times 10^{2}/5.0 \times 10^{9}$		
$C_2H_5COC_2H_5(+M) \leftrightarrow CH_3 + C_2H_5COCH_2(+M)$	k_{inf}	1.37×10^{21}	−1.36	82 700
	k_0	4.88×10^{104}	−25.50	105 300
α,T^{***},T^* and T^{**}		$0.62/1.5 \times 10^{3}/1.2 \times 10^{2}/5.0 \times 10^{9}$		
$C_2H_5COC_2H_5 + OH \leftrightarrow C_2H_5COC_2H_4p + H_2O$		1.06×10^{10}	0.97	1593
$C_2H_5COC_2H_5 + OH \leftrightarrow C_2H_5COC_2H_4s + H_2O$		5.20×10^{03}	2.77	−1230
$C_2H_5COC_2H_5 + H \leftrightarrow C_2H_5COC_2H_4p + H_2$		1.33×10^{06}	2.54	6760
$C_2H_5COC_2H_5 + H \leftrightarrow C_2H_5COC_2H_4s + H_2$		1.91×10^{06}	2.29	2880
$C_2H_5COC_2H_5 + O_2 \leftrightarrow C_2H_5COC_2H_4p + HO_2$		6.00×10^{13}	0.00	52 300
$C_2H_5COC_2H_5 + O_2 \leftrightarrow C_2H_5COC_2H_4s + HO_2$		4.04×10^{13}	0.00	45 900
$C_2H_5COC_2H_5 + CH_3 \leftrightarrow C_2H_5COC_2H_4p + CH_4$		3.06×10^{00}	3.65	7150
$C_2H_5COC_2H_5 + CH_3 \leftrightarrow C_2H_5COC_2H_4s + CH_4$		1.70×10^{01}	3.28	5270
$C_2H_5COC_2H_5 + HO_2 \leftrightarrow C_2H_5COC_2H_4p + H_2O_2$		2.72×10^{01}	3.59	17 200
$C_2H_5COC_2H_5 + HO_2 \leftrightarrow C_2H_5COC_2H_4s + H_2O_2$		6.88×10^{12}	0.05	17 900
$C_2H_5COC_2H_5 + C_2H_3 \leftrightarrow C_2H_5COC_2H_4p + C_2H_4$		1.00×10^{12}	0.00	10 400
$C_2H_5COC_2H_5 + C_2H_3 \leftrightarrow C_2H_5COC_2H_4s + C_2H_4$		6.00×10^{11}	0.00	5600
$C_2H_5COC_2H_5 + C_2H_5 \leftrightarrow C_2H_5COC_2H_4p + C_2H_6$		1.00×10^{11}	0.00	13 400
$C_2H_5COC_2H_5 + C_2H_5 \leftrightarrow C_2H_5COC_2H_4s + C_2H_6$		6.00×10^{10}	0.00	8600
$C_2H_5COC_2H_5 + CH_3O \leftrightarrow C_2H_5COC_2H_4p + CH_3OH$		4.34×10^{11}	0.00	6460
$C_2H_5COC_2H_5 + CH_3O \leftrightarrow C_2H_5COC_2H_4s + CH_3OH$		1.15×10^{12}	0.00	4570
$C_2H_5COC_2H_5 + CH_3O_2 \leftrightarrow C_2H_5COC_2H_4p + CH_3O_2H$		9.20×10^{-01}	3.97	18 300
$C_2H_5COC_2H_5 + CH_3O_2 \leftrightarrow C_2H_5COC_2H_4s + CH_3O_2H$		6.88×10^{12}	0.05	17 900
$C_2H_5COC_2H_4p \leftrightarrow C_2H_5COC_2H_4s$		4.35×10^{10}	0.87	37 018
$C_2H_5COC_2H_4p \leftrightarrow C_2H_5CO + C_2H_4$		7.17×10^{13}	−1.93	26 258
$C_2H_5COC_2H_4s \leftrightarrow C_2H_5COC_2H_3 + H$		8.70×10^{16}	−0.82	42 100
$C_2H_5COC_2H_4s \leftrightarrow CH_3CHCO + C_2H_5$		1.21×10^{19}	0.42	42 727

cases ($\phi = 0.5$), where it is slower by a factor of 2 at lower temperatures.

Recently, Davidson et al.[56] performed shock tube measurements on some *n*-alkanes and oxygenates, among which a stoichiometric 3-pentanone/Ar mixture at $1170 < T < 1300$ K and a reflected shock pressure of around 1.7−1.8 atm was treated. These data are also shown in Figure 4. Even though a direct comparison cannot be made between their data and the data presented in this study, given that mixture compositions are different, both experiments seem to show similar activation energies over the temperature range studied.

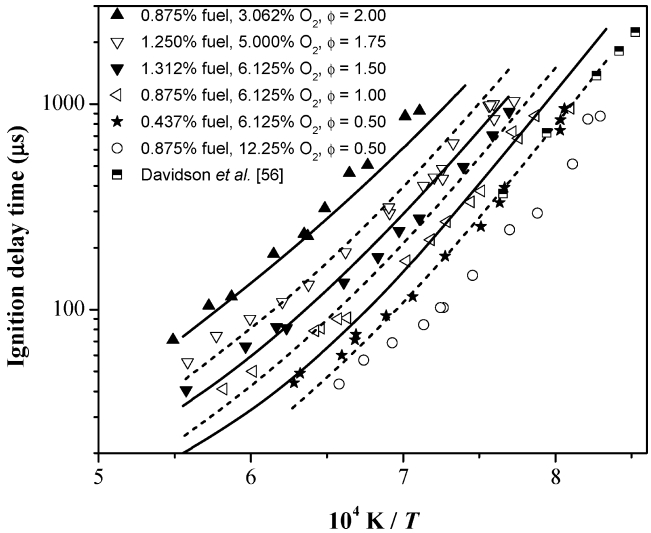

Figure 4. Ignition delay times of all 3-pentanone/O_2/Ar mixtures given in Table 2 at a reflected shock pressure of 1 atm. (symbols: experiment, lines: model calculation). Davidson et al. data normalized to 1 atm, $\phi = 1.0$, 0.57% 3-pentanone, 4.0% O_2 in Ar.[56]

A multiple regression analysis has been performed in the high temperature regime and a canonical expression defining the experimental ignition delay time of 3-pentanone has been obtained:

$$\tau/\mu s = 2.96 \times 10^{-3} \times (\text{fuel})^{0.50\pm0.11}(O_2)^{-1.53\pm0.55} \times \exp(16\,480 \pm 390/T) \quad (6a)$$

Similarly a canonical expression is derived based on model results:

$$\tau/\mu s = 1.41 \times 10^{-3} \times (\text{fuel})^{0.64\pm0.18}(O_2)^{-1.44\pm0.08} \times \exp(18\,220 \pm 500/T) \quad (6b)$$

Given that all the experiments were carried out at constant pressure, this factor is neglected in both expressions; the diluent (Ar) effect was also neglected, given that it varied over a narrow range: 87−96%.

The expressions above suggest that the model predicts a slightly higher dependence of the ignition delay time on fuel concentration and comparable dependence (−1.44 vs −1.53) on O_2. Moreover, the model predicts an activation energy about 10% higher than the experimental one, indicating a very good agreement between the model and experiment.

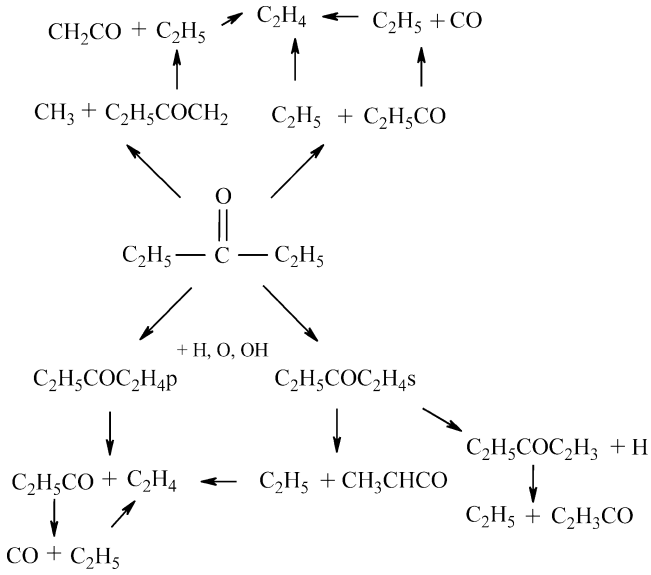

Figure 5. Simplified oxidation scheme of 3-pentanone.

To be able to compare the three ketones in terms of the reactivity they exhibit, a similar analysis has been performed for 2-butanone eq 7 and acetone eq 8 based on the shock tube ignition delay time data,[1,2] and the following expressions are obtained:

$$\tau/\mu s = 8.15 \times 10^{-3} \times (\text{fuel})^{0.50\pm0.07}(O_2)^{-1.39\pm0.05} \times \exp(18\,630 \pm 420/T) \quad (7)$$

$$\tau/\mu s = 6.07 \times 10^{-3} \times (\text{fuel})^{0.77\pm0.07}(O_2)^{-1.26\pm0.05} \times \exp(20\,920 \pm 430/T) \quad (8)$$

Acetone shows the strongest dependence on fuel concentration and has a somewhat lesser dependency on O_2 content. On the other hand, 2-butanone and 3-pentanone show very similar

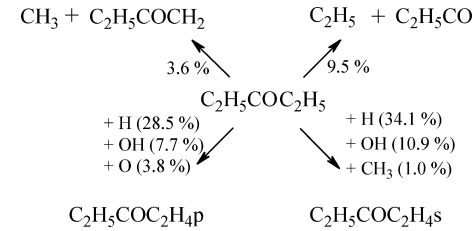

Figure 7. Flux analysis for mixture 3 at 1250 K and 20% fuel conversion.

dependencies and hence are quite similar in terms of reactivity as well as for observed laminar flame speed results, which will be covered in detail in the coming section.

Unimolecular decompositions of 3-pentanone yields methyl (CH_3), 2-methyl carbonyl ($C_2H_5COCH_2$), ethyl (C_2H_5), and propionyl (C_2H_5CO) radicals, which makes the fate of the ethyl radical and hence ethylene/vinyl chemistry very important for this system in terms of ignition delay times as well as laminar flame speeds, which will be discussed in the coming section. Abstraction of hydrogen atom from the parent fuel leads to the formation of fuel radicals $C_2H_5COC_2H_4p$ and $C_2H_5COC_2H_4s$. β-scission of the former radical results in the formation of ethylene and propionyl radical, whereas the latter mostly decomposes into methyl ketene and ethyl radical, Figure 5.

A brute force ignition delay time sensitivity analysis was performed for mixture 4 at 1400 K and is given in Figure 6. However, the most sensitive high temperature chain branching reaction $H + O_2 \rightarrow O + OH$ is omitted on the plot for the sake of clarity. Each reaction was tested by multiplying (k^+) and dividing (k^-) both the forward and reverse rate constants by a factor of 2, without affecting the equilibrium, and recording the resulting ignition delay time (τ^+ and τ^-). Reactions with a negative logarithmic sensitivity coefficient promote reactivity, whereas ones with positive coefficients are inhibiting. The first five reactions on the sensitivity plot compete with the chain branching reaction $H + O_2 \rightarrow O + OH$ for H atoms and hence inhibit overall reactivity. Unimolecular decomposition of the

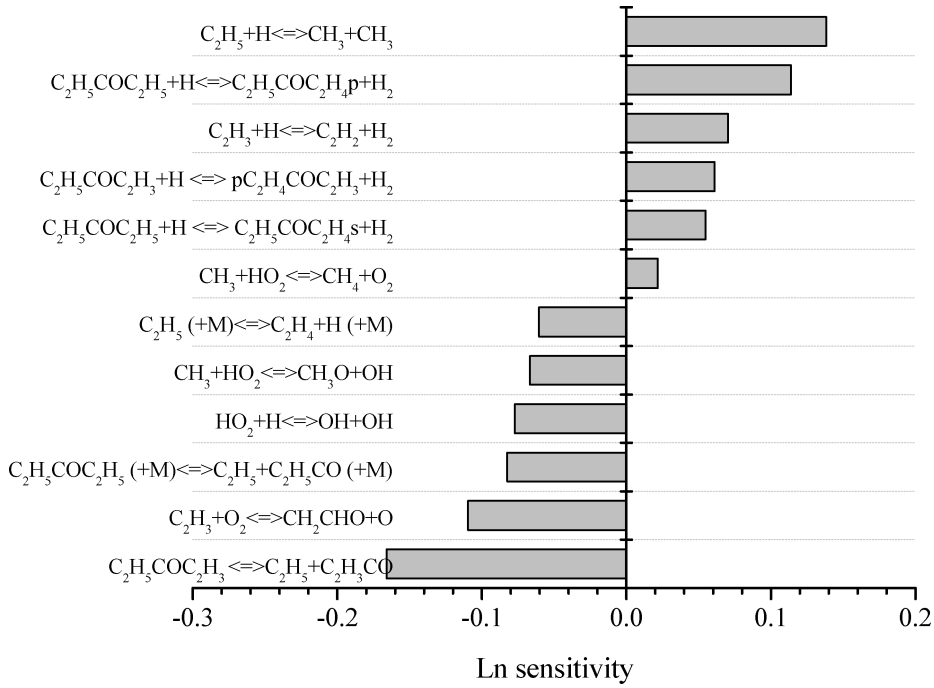

Figure 6. Ignition delay time sensitivity analysis (1400 K, $\varphi = 1.0$, 0.875% fuel, 6.125% O_2).

TABLE 6: Experimental Results and Equilibrium Parameters for 2-Butanone/Air

T_i (°C)	ϕ	V_s^0 (mm s^{-1})	wrinkles	P_m (bar)	P_{AICC} (bar)	σ	S_l^0 (mm s^{-1})	L (mm)
31.7	1.102	3166.3	no	8.80	9.57	8.106	390.6	0.81
31.4	1.299	2699.7	no	8.88	9.63	7.959	339.2	0.23
31.6	1.200	3086.4	no	8.84	9.65	8.056	383.1	0.67
31	0.898	2626.4	no	8.40	9.00	7.610	345.1	1.67
31.8	1.052	3152.3	no	8.80	9.47	8.071	390.6	1.15
31	1.013	2987.1	no	8.72	9.40	8.019	372.5	0.92
31.8	0.952	2837.6	no	8.50	9.17	7.810	363.3	1.21
31.9	1.150	3084.0	no	8.84	9.62	8.087	381.4	0.67
32	1.248	2816.5	no	8.84	9.64	8.000	352.1	0.17
30.7	0.753	1778.7	no	7.82	8.23	6.844	259.9	1.98
31.2	0.849	2384.8	no	8.24	8.74	7.365	323.8	1.71
32.1	1.351	2448.2	yes	8.85	9.57	7.883	310.6	0.20
32.1	1.078	3174.8	no		9.52	8.088	392.5	1.06
32.7	0.802	2113.6	no	7.97	8.46	7.085	298.3	1.87
30.9	1.398	2164.3	yes	8.74	9.57	7.857	275.5	−0.06
32	1.090	3273.2	no	8.74	9.55	8.096	404.3	1.28
32.9	1.098	3195.8	no	8.79	9.54	8.076	395.7	1.07
32.6	0.899	2611.2	no	8.35	8.94	7.575	344.7	1.93
33.6	1.150	3174.2	no	8.84	9.57	8.046	394.5	0.89
33.9	1.298	2707.8	no	8.78	9.56	7.902	342.7	0.24
34.8	0.750	1732.6	no	7.69	8.11	6.745	256.9	1.47
35.4	1.099	3183.4	no	8.74	9.46	8.016	397.1	0.78
36	1.118	3209.4	no	8.75	9.51	8.001	401.1	1.14

TABLE 7: Experimental Results and Equilibrium Parameters for 3-Pentanone/Air

T_i (°C)	ϕ	V_s^0 (mm s^{-1})	wrinkles	P_m (bar)	P_{AICC} (bar)	σ	S_l^0 (mm s^{-1})	L (mm)
31.0	1.148	3448.0	limited	9.04	9.70	8.146	423.3	1.19
31.3	1.248	3137.6	limited	9	9.71	8.054	389.6	0.51
32.2	1.348	2830.4	limited	8.9	9.63	7.923	357.2	0.23
30.7	0.850	2515.0	no	8.34	8.80	7.402	339.8	2.10
31.7	1.001	3265.9	no	8.77	9.39	8.003	408.1	1.81
32.6	0.792	2119.3	no	8.11	8.54	7.046	300.8	2.25
31.4	1.248	3247.0	limited	8.96	9.71	8.051	403.3	0.75
31.9	1.050	3349.4	limited	8.89	9.51	8.099	413.6	1.28
32.9	1.350	2597.9	limited	8.85	9.59	7.904	328.7	−0.20
30.9	0.969	3109.8	no	8.67	9.30	7.924	392.5	1.66
32.0	0.899	2677.0	no	8.34	9.00	7.618	351.4	2.15
32.5	0.750	1820.4	no	7.71	8.18	6.800	267.7	2.49
33.1	1.450	2191.6	yes	8.95	9.49	7.785	281.5	−0.01
32.2	1.130	3432.3	limited	8.96	9.63	8.125	422.4	1.17
32.9	1.170	3378.5	limited	8.95	9.65	8.086	417.8	0.97
29.9	0.939	2918.8	no	8.52	9.23	7.837	372.5	1.76
31.0	0.933	2953.7	no	8.46	9.16	7.785	379.4	1.87
31.0	1.076	3459.7	no	8.8	9.60	8.148	424.6	1.46
31.5	1.053	3444.0	no	8.8	9.53	8.113	424.5	1.50
31.3	1.204	3233.8	limited	8.96	9.72	8.097	399.4	0.93
31.4	1.297	3102.5	limited	8.9	9.70	7.999	387.8	0.85
32.3	1.397	2307.9	limited	9.02	9.58	7.863	293.5	0.06

fuel and of ethyl vinyl ketone supply ethyl radicals to the pool forming ethylene and hydrogen, which speeds up ignition.

A fuel decomposition pathway analysis is given below for mixture 3 (1.3125% fuel, 6.125% O_2, $\phi = 1.5$) at 1250 K.

At the conditions given above, most of the fuel conversion takes place through hydrogen abstraction mainly by H atom and OH radicals. Both fuel radicals are produced in comparable quantities, and 13% of the fuel goes through unimolecular decomposition.

Laminar Flame Speeds. The evolution of the radius versus time was determined for each run. By applying a multiple regression analysis, according to eq 5, both V_s^0 and L were obtained with a coefficient of determination r^2 better than 0.999. Equilibrium calculations have also been performed in order to derive the expansion factor and P_{AICC}. The results are summarized in Tables 6 and 7.

Laminar flame speed calculations are carried out using the PREMIX module of the same application.[51] Multicomponent transport and thermal diffusion effects were taken into account in the calculations. A maximum of 1500 grid points are allowed, and CURV and GRAD values of 0.02 were attained, ensuring that the final solution was independent of the number of grid points.

Experimental and simulation results are given in Figure 8 for all three ketones. 2-Butanone and 3-pentanone laminar flame speeds are a result of this study, whereas acetone was published earlier by Pichon et al.,[1] and all are plotted here for comparison in terms of reactivity. These acetone flame speed measurements are in very good agreement with the recent study of Konnov et al.[57] in which a completely different approach was employed (heat flux method) for measuring laminar flame speeds. Acetone, among all, shows the least reactivity with a peak value that is 20% smaller than that of 3-pentanone, which is the most reactive ketone in this case. Acetone yields acetonyl (CH_3COCH_2) radical most significantly via hydrogen abstraction by H and OH in flame conditions. Through beta-scission of acetonyl radical to ketene (CH_2CO) and a methyl radical, $CH_3COCH_2 \rightarrow CH_3 + CH_2CO$, the following reactions occur introducing more CH_3 radical and HCCO to the system. Although methyl radicals recombine to give ethane, the following reactions occur between ketene and H atoms:

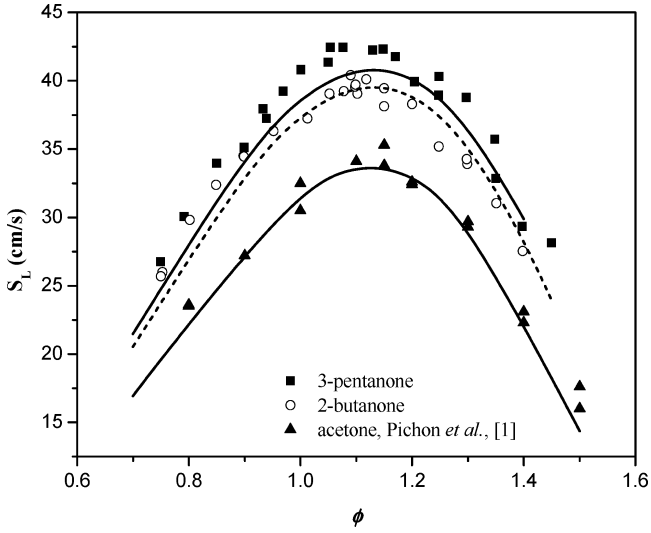

Figure 8. Laminar flame speed of all ketones studied, $P = 1$ atm, $T_i = 305$. Acetone flame speed data[1] are at 1 atm, as well as 2-butanone and 3-pentanone. (symbols: experiment, lines: model calculation).

$$CH_2CO + H \leftrightarrow HCCO + H_2 \quad (R3)$$

$$CH_2CO + H \leftrightarrow CH_3 + CO \quad (R4)$$

Increasing the temperature increases the rates of R3 and R4, which altogether results in acetone flame speeds being significantly lower than both 2-butanone and 3-pentanone, which show similar reactivity, with the latter being slightly more reactive due to its two ethyl groups forming ethylene and hydrogen (R7) as opposed to a less reactive methyl radical.

$$C_2H_5COC_2H_4p \leftrightarrow C_2H_5CO + C_2H_4 \quad (R5)$$

$$C_2H_5CO \leftrightarrow C_2H_5 + CO \quad (R6)$$

$$C_2H_5(+M) \leftrightarrow C_2H_4 + H(+M) \quad (R7)$$

On one hand, 3-pentanone is consumed by hydrogen abstraction yielding the fuel radical $C_2H_5COC_2H_4p$, which yields ethyl radical via R5 and R6, which increases the H-atom concentration by decomposing into ethylene and hydrogen atom and hence promotes the high temperature chain branching reaction $H + O_2 \leftrightarrow O + OH$.

On the other hand, decomposition of the fuel radical $C_2H_5COC_2H_4s$ resulting from the abstraction of a hydrogen atom alpha to the carbonyl carbon which decomposes into methyl ketene (CH_3CHCO) and ethyl radical through R8.

$$C_2H_5COC_2H_4s \leftrightarrow CH_3CHCO + C_2H_5 \quad (R8)$$

$$CH_3CHCO + H \leftrightarrow C_2H_5CO \quad (R9)$$

$$CH_3CHCO + OH \leftrightarrow C_2H_5 + CO_2 \quad (R10)$$

At high temperatures, the reaction of CH_3CHCO with H atoms is more important than its reaction with OH, therefore eq R9 competes with the high temperature chain branching reaction $H + O_2 \leftrightarrow O + OH$ for H atoms, which makes this path more inhibiting. Therefore, branching ratios of the hydrogen abstraction reactions from 3-pentanone, especially by H atom and OH radical, are very important in determining the reactivity correctly in freely propagating flame conditions, even though these reactions did not show up in the sensitivity analysis; Figure 9.

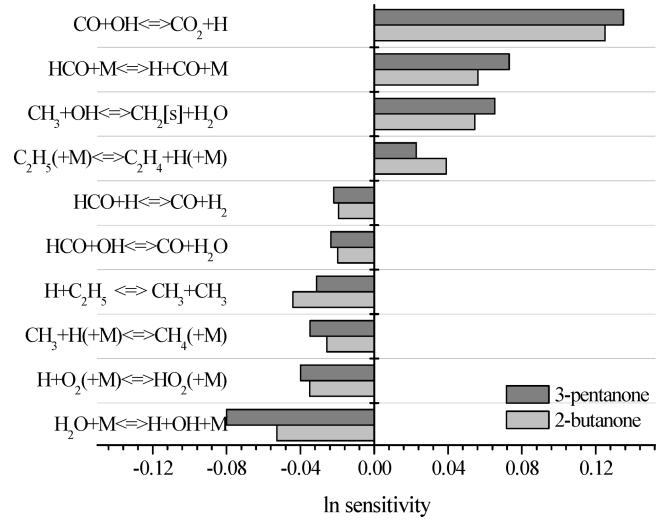

Figure 9. Flame speed sensitivity for 2-butanone and 3-pentanone flames at $\Phi = 1.0$, $T = 298$ K, $P = 1$ atm.

Similarly, 2-butanone decomposes through hydrogen abstraction by H and OH in the given flame conditions:

$$C_2H_5COCH_3 + H \leftrightarrow CH_3CHCOCH_3 + H_2 \quad (R11)$$

$$C_2H_5COCH_3 + H \leftrightarrow CH_2CH_2COCH_3 + H_2 \quad (R12)$$

$$C_2H_5COCH_3 + OH \leftrightarrow CH_3CHCOCH_3 + H_2O \quad (R13)$$

$$C_2H_5COCH_3 + OH \leftrightarrow CH_2CH_2COCH_3 + H_2O \quad (R14)$$

$$CH_3CHCOCH_3 \leftrightarrow CH_3CHCO + CH_3 \quad (R15)$$

$$CH_2CH_2COCH_3 \leftrightarrow CH_3CO + C_2H_2 \quad (R16)$$

$$CH_3CO(+M) \leftrightarrow CH_3 + CO(+M) \quad (R17)$$

Depending on the branching ratio of hydrogen abstraction reactions as well as decomposition of the fuel radicals, 2-butanone yields methyl ketenes like 3-pentanone, which supply ethyl radicals via eqs R9 and R10. Acetyl radical, on the other hand decomposes to methyl and CO, which makes the relative rate constants of these reactions important for fuel reactivity estimations, and the simulations agree well with the experimental data.

Flame speed sensitivity analyses for 2-butanone and 3-pentanone are given on Figure 9. For both fuels, the high temperature chain branching reaction $H + O_2 \leftrightarrow O + OH$ is again the most sensitive, promoting reactivity for laminar flame speeds as well as ignition delay times; however, it is omitted

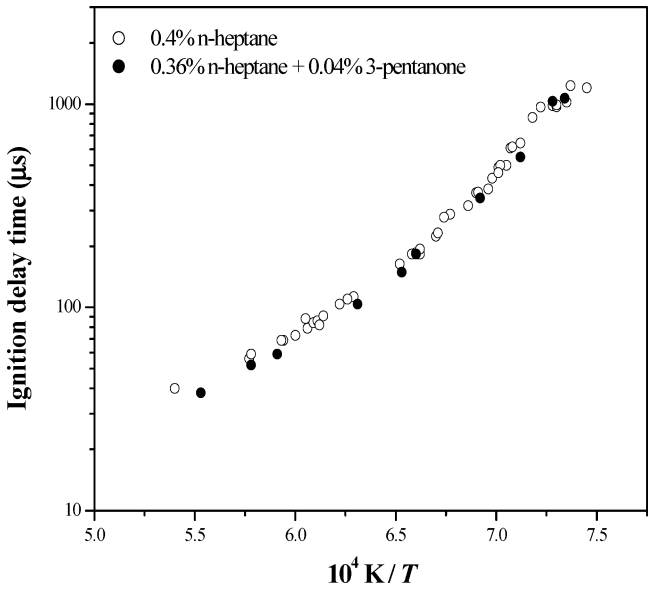

Figure 10. Ignition delay times for *n*-heptane and *n*-heptane/3-pentanone in O_2/Ar at 1 atm. Fuel compositions: (○) 100% *n*-heptane: (●) 15% 3-pentanone/85% *n*-heptane.

on the plot below as on Figure 4 for the sake of clarity. Analysis shows more sensitivity to H_2/O_2 and small hydrocarbon chemistry than to the decomposition chemistry of the parent fuel. Therefore, the accuracy of the C0−C2 chemistry affects flame speed calculations more than the submechanisms of each individual fuel. On the other hand, even though fuel decompositions reactions do not show up in the sensitivity plot, they determine the accuracy in getting the radical pool correct, as outlined previously. The extent to which hydrogen abstraction from the fuel by H atom competes with the chain branching reaction does have a small effect on the flame speed. In the cases studied here, methyl and ethyl radicals are produced directly from unimolecular decomposition of the fuel. Ignition delay time calculations show that these rate constants perform well in shock tube ignition delay time predictions.

Calculations show good agreement overall, capturing the peak points that occur around $\phi \sim 1.15$ for all three fuels. There is less than 10% under-prediction on the lean side for both 2-butanone and 3-pentanone. As shown in Figure 9, both fuels are sensitive to the same reactions and show very similar sensitivity coefficients. In addition to the common plot, 2-butanone also shows some sensitivity to the methyl recombination reaction generating ethane, $CH_3 + CH_3 (+M) \rightarrow C_2H_6 (+M)$, due to its methyl group attached to the carbonyl carbon, inhibiting overall reactivity.

Addition of the Fuel Tracer to n-Heptane. An important criterion in the choice of a fuel tracer is that it must not alter the burning characteristics of the main fuel. In order to ascertain whether 3-pentanone influences the combustion of *n*-heptane, shock tube ignition delay measurements have been taken for an *n*-heptane/O_2/Ar mixture and directly compared to another mixture with the same O_2 and Ar content but by replacing 15% of the fuel with 3-pentanone, Figure 10.

Ignition delay characteristics of *n*-heptane remained unaffected by the addition of 3-pentanone in concentrations up to 15%; similar results were obtained for acetone and 2-butanone.[1,2] Therefore, the addition of up to 15 mol % of 3-pentanone to *n*-heptane does not appear to influence the combustion chemistry. Of course, if much larger amounts of the fuel tracer are added, then the chemistry of the tracer itself may become more significant. Hong et al.[13] have investigated the effect of oxygenate addition, among which 3-pentanone is included, to *n*-heptane on soot yield in a high pressure shock tube and at a similar temperature range as of this study; 1500−1900 K. They found that soot yield decreased with the addition of oxygenates in fuel-rich mixtures of *n*-heptane.

Conclusions

Shock tube ignition delay times have been measured for 3-pentanone, and a kinetic submechanism has been developed. Laminar flame speed measurements have been taken in a spherical bomb for both 3-pentanone and 2-butanone, and results are presented in comparison with acetone in order to have a complete view on the reactivity of these ketones. 3-Pentanone, even though it is the largest molecule among all, shows the highest reactivity due to the two ethyl groups attached to the carbonyl carbon. 2-Butanone bears one methyl and one ethyl groups and is slightly less reactive. Acetone is the least reactive, given that it produces more methyl radicals that recombine into ethane, thus slowing down the overall reactivity in the conditions studied. This behavior is also quantified by canonical expressions relating experimental ignition delay times to fuel and oxygen concentrations as well as temperature. The kinetic mechanism is in good agreement with experimental data and is able to capture peak burning velocity trends.

3-Pentanone has been tested with *n*-heptane by replacing 15% of the fuel with the tracer, and it has been observed that addition of the tracer to the given extent did not alter the oxidation characteristics of the parent fuel, which is an important criterion, among others, in choosing the tracer.

Acknowledgment. Financial support from Science Foundation Ireland (SFI) under grant number 07/RFP/CHEF845 and the Irish Research Council for Science, Engineering and Technology (IRCSET) for an Embark Fellowship are gratefully acknowledged. Z. S. would like to thank Dr. Wayne K. Metcalfe and Dr. Stephen Dooley for insightful discussions. This study was partially supported by the ULYSSES program of the French Ministry of Foreign Affairs No. 19848RK.

Supporting Information Available: The detailed chemical kinetic mechanism (jp107167f_si_001.txt) and thermochemical data (jp107167f_si_002.txt) are available as Supporting Information. This material is available free of charge via the Internet at http://pubs.acs.org.

References and Notes

(1) Pichon, S.; Black, G.; Chaumeix, N.; Yahyaoui, M.; Simmie, J. M.; Curran, H. J.; Donohue, R. *Combust. Flame* **2009**, *156*, 494–504.
(2) Serinyel, Z.; Black, G.; Curran, H. J.; Simmie, J. M. *Combust. Sci. Technol.* **2010**, *182*, 574–587.
(3) Schulz, C.; Sick, V. *Prog. Energy Combust. Sci.* **2005**, *31*, 75–121.
(4) Berckmüller, M.; Tait, N. P.; Lockett, R. D.; Greenhalgh, D. A.; Kiyoshi, I.; Urata, Y.; Umiyama, H.; Yoshida, K. *Proc. Combust. Inst.* **1994**, *25*, 151–156.
(5) Modica, V.; Morin, C.; Guibert, P. *Appl. Phys. B: Laser Opt.* **2007**, *87*, 193–204.
(6) Koch, J. D.; Hanson, R. K.; Koban, W.; Schulz, C. *Appl. Opt.* **2004**, *43*, 5901–5910.
(7) Einecke, S.; Schultz, C.; Sick, V. *App. Phys. B: Lasers Opt.* **2000**, *71*, 717–723.
(8) Neij, H.; Johansson, B.; Aldén, M. *Combust. Flame* **1994**, *99*, 449–457.
(9) Han, D.; Steeper, R. R. *Proc. Combust. Inst.* **2002**, *29*, 727–734.
(10) Rothamer, D. A.; Snyder, J. A.; Hanson, R. K.; Steeper, R. R. *Appl. Phys. B* **2010**, *99*, 371–384.
(11) Decottignies, V.; Gasnot, L.; Pauwels, J. *Combust. Flame* **2002**, *130*, 225–240.

(12) Davidson, D. F.; Herbon, J. T.; Horning, D. C.; Hanson, R. K. *Int. J. Chem. Kinet.* **2001**, *33*, 775–783.
(13) Hong, Z.; Davidson, D. F.; Vasu, S. S.; Hanson, R. K. *Fuel* **2009**, *88*, 1901–1906.
(14) Smith, J. M.; Simmie, J. M.; Curran, H. J. *Int. J. Chem. Kinet.* **2005**, *37*, 728–736.
(15) Morley, C., Gaseq available from http://www.arcl02.dsl.pipex.com/gseqrite.htm.
(16) Lamoureux, N.; Djebaili-Chaumeix, N.; Paillard, C. E. *Exp. Therm. Fluid Sci.* **2003**, *27*, 385–393.
(17) Eschenbach, R. C.; Agnew, J. T. *Combust. Flame* **1958**, *2*, 273–285.
(18) Bradley, D.; Gaskell, P. H.; Gu, X. J. *Combust. Flame* **1996**, *104*, 176–198.
(19) Bradley, D.; Hicks, R. A.; Lawes, M.; Sheppard, C. G. W.; Woolley, R. *Combust. Flame* **1998**, *115*, 126–144.
(20) Clavin, P. *Prog. Energy Combust. Sci.* **1985**, *11*, 1–59.
(21) Matalon, M.; Matkowsky, B. J. *J. Fluid Mech.* **1982**, *124*, 239–259.
(22) Law, C. K.; Sung, C. J. *Prog. Energy Combust. Sci.* **2000**, *26*, 459–505.
(23) Dubois, T.; Chaumeix, N.; Paillard, C. E. *Energy Fuels* **2009**, *23*, 2453–2466.
(24) Yahyaoui, A.; Djebaili-Chaumeix, N.; Dagaut, P.; Paillard, C. E. *Energy Fuels* **2008**, *22*, 3701–3708.
(25) The Combustion Simulation Laboratory, www.softpredict.com; Rotexo GmbH & Co.: KG, Haan, Germany, 2010.
(26) Petersen, E. L.; Kalitan, D. M.; Simmons, S.; Bourque, G.; Curran, H. J.; Simmie, J. M. *Proc. Combust. Inst.* **2007**, *31*, 447–454.
(27) Gallagher, S.; Curran, H. J.; Metcalfe, W. K.; Healy, D.; Simmie, J. M.; Bourque, G. *Combust. Flame* **2008**, *153*, 316–333.
(28) Healy, D.; Curran, H. J.; Dooley, S.; Simmie, J. M.; Kalitan, D. M.; Petersen, E. L.; Bourque, G. *Combust. Flame* **2008**, *155*, 451–461.
(29) Healy, D.; Curran, H. J.; Simmie, J. M.; Kalitan, D. M.; Zinner, C. M.; Barrett, A. B.; Petersen, E. L.; Bourque, G. *Combust. Flame* **2008**, *155*, 441–448.
(30) Healy, D.; Kalitan, D. M.; Aul, C. J.; Petersen, E. L.; Bourque, G.; Curran, H. J. *Energy Fuels* **2010**, *24*, 1521–1528.
(31) Healy, D.; Kopp, M. M.; Polley, N. L.; Petersen, E. L.; Bourque, G.; Curran, H. J. *Energy Fuels* **2010**, *24*, 1617–1627.
(32) Healy, D.; Donato, N. S.; Aul, C. J.; Petersen, E. L.; Zinner, C. M.; Bourque, G.; Curran, H. J. *Combust. Flame* **2010**, *157*, 1526–1539.
(33) Healy, D.; Donato, N. S.; Aul, C. J.; Petersen, E. L.; Zinner, C. M.; Bourque, G.; Curran, H. J. *Combust. Flame* **2010**, *157*, 1540–1551.
(34) C4 mechanism NUI Galway available from http://c3.nuigalway.ie/.
(35) Ritter, E. R.; Bozzelli, J. W. *Int. J. Chem. Int. J. Chem. Kinet.* **1991**, *23*, 767–778.
(36) Tsang, W.; Hampson, R. F. *J. Phys. Chem. Ref. Data* **1986**, *15*, 1087–1280.
(37) Tsang, W. *Combust. Flame* **1989**, *78*, 71–86.
(38) Dean, A. M. *J. Phys. Chem.* **1985**, *89*, 4600–4608.
(39) Dean, A. M.; Bozzelli, J. W.; Ritter, E. R. *Combust. Sci. Technol.* **1991**, *80*, 63–85.
(40) Gilbert, R. G.; Luther, K.; Troe, J. *J. Ber. Bunsengesellschaft/Phys. Chem. Chem. Phys.* **1982**, *87*, 169–177.
(41) Orme, J.; Curran, H. J.; Simmie, J. M. *J. Phys. Chem. A* **2006**, *110*, 114–131.
(42) Aguilera-Iparraguirre, J.; Curran, H. J.; Klopper, W.; Simmie, J. M. *J. Phys. Chem. A* **2008**, *112*, 7047–7054.
(43) Carstensen, H.-H.; Dean, A. M. *Proc. Comb. Inst.* **2005**, *30*, 995–1003.
(44) Seakins, P. W.; Pilling, M. J.; Niiranen, J. T.; Gutman, D.; Krasnoperov, L. N. *J. Phys. Chem.* **1992**, *96*, 9847–9855.
(45) Curran, H. J. *Int. J. Chem. Kinet.* **2006**, *38*, 250–275.
(46) Saeys, M.; Reyniers, M. F.; Marin, G. B.; Van Speybroeck, V.; Waroquier, M. *AIChE J.* **2004**, *50*, 426–444.
(47) Huynh, L. K.; Lin, K. C.; Violi, A. *J. Phys. Chem. A* **2008**, *112*, 13470–13480.
(48) Seiser, H.; Pitsch, H.; Seshadri, K.; Pitz, W. J.; Curran, H. J. *Proc. Combust. Inst.* **2000**, *28*, 2029–2037.
(49) Huynh, L. K.; Violi, A. *J. Org. Chem.* **2008**, *73*, 94–101.
(50) Matheu, D. M.; Green, W. H., Jr.; Grenda, J. M. *Int. J. Chem. Kinet.* **2003**, *35*, 95–119.
(51) CHEMKIN-PRO; Reaction Design: San Diego, California, USA, 2008.
(52) Metcalfe, W. K.; Pitz, W. J.; Curran, H. J.; Simmie, J. M.; Westbrook, C. K. *Proc. Combust. Inst.* **2007**, *31*, 377–384.
(53) Gaïl, S.; Dagaut, P.; Black, G.; Simmie, J. M. *Combust. Sci. Technol.* **2008**, *180*, 1748–1771.
(54) Kim, K.; Shin, K. S. *Bull. Korean Chem. Soc.* **2001**, *22*, 303–307.
(55) Oehlschlaeger, M. A.; Davidson, D. F.; Herbon, J. T.; Hanson, R. K. *Int. J. Chem. Kinet.* **2004**, *36*, 67–78.
(56) Davidson, D. F.; Ranganath, S. C.; Lam, K. Y.; Liaw, M.; Hong, Z.; Hanson, R. K. *J. Prop. Power* **2010**, *26*, 280–287.
(57) Konnov, A. A.; Meuwissen, R. J.; de Goey, L. P. H. Joint Meeting of the Scandinavian-Nordic and French Sections of the Combustion Institute, Copenhagen, November 9−10, 2009.
(58) Lowry, W. B.; Serinyel, Z.; Krejci, M.; Curran, H. J.; Bourque, G.; Petersen, E. L. *Proc. Combust. Inst.* **2011**, *33*, DOI:10.1016/j.proci.2010.05.042.
(59) Zhou C.-W., Simmie J. M., Curran H. J., Ab initio and Kinetic Study of the Reaction of Ketones with OH. Part I: Hydrogen-Abstraction from $H_3CC(O)CH_{3-x}(CH_3)_x$, $x = 0 \rightarrow 2$, by OH, in review.

JP107167F